Journal of Archaeological Science 181 (2025) 106297

Contents lists available at ScienceDirect

Journal of Archaeological Science

journal homepage: www.elsevier.com/locate/jas

Shipwreck detection in bathymetry data using semi-automated methods: Combining machine learning and topographic inference approaches

Cal T. Pols [a,*], Fraser Sturt [a], Crystal El Safadi [a], Antonia Marcu [b]

[a] Department of Archaeology, University of Southampton, Southampton, United Kingdom
[b] Department of Electronics and Computer Science, University of Southampton, Southampton, United Kingdom

ARTICLE INFO

Dataset link: https://seabed.admiralty.co.uk/, https://www.admiralty.co.uk/access-data/marine-data, https://github.com/Esri/deep-learning-frameworks

Keywords:
Shipwrecks
Machine learning
Bathymetry
Remote sensing
Maritime archaeology
Geographic Information Systems (GIS)

ABSTRACT

This research presents a workflow that integrates emerging machine learning methods with geospatial mapping techniques to improve the identification of shipwrecks in bathymetry data. By first refining the study area into high-potential units, machine learning algorithms can be applied more efficiently. This approach accelerates the process, reduces computational demands, and offers an adaptive method that can eventually be tailored to survey needs and different seabed environments. This paper contributes to the current discourse surrounding the discovery and management of underwater cultural heritage (UCH) in the context of global seabed mapping, developments in autonomous marine survey, and continued offshore development. Shipwrecks constitute a significant proportion of UCH sites that are increasingly likely to be discovered and impacted by these developments, and thus archaeologists need adequate tools for their rapid detection and monitoring to keep pace with the rate of data generation.

The proposed workflow uses a raster extraction method as a filtering process to identify areas of seabed with high shipwreck potential, based on their topographic signature in three different visualisations of bathymetry (slope, curvature, and topographic position index). Using these results, several different machine learning algorithms were tested on their ability to identify both intact, visible shipwrecks ('conspicuous' wrecks) as well as smaller, possible wreck sites. These methods were tested over an area of 3,131 km^2 from the south coast of England. Results show that the Raster Extraction method was able to filter out 96% of the test data, while still detecting 78% of the test shipwrecks (n=253). Machine learning models trained on different data visualisations (Hillshade, Shaded Relief, Curvature) and algorithms (Single Shot Detector, Faster R-CNN, and Mask R-CNN) had varied performances in terms of recall and precision.

1. Introduction

UNESCO (2007, 4) have estimated that there are likely to be in excess of three million shipwrecks world wide. The location and attribution of the majority of these remains to be resolved. While underwater cultural heritage (UCH; UNESCO, 2001) is not limited to shipwrecks, these sites often have a legislative, research, and commercial focus, as they are typically some of the most visible and evocative sites on the sea floor. Shipwrecks are an important resource not only in terms of their historical and archaeological potential, but also for their wider socio-cultural value (Adams, 2001, 2013; Gibbins and Adams, 2001). As such, the significance of shipwrecks has been well recognised in maritime archaeology since the early stages of the discipline (Basch, 1972; Hasslöf, 1972; Muckelroy, 1978).

Today, shipwrecks represent both an opportunity and a challenge. An opportunity to deepen our understanding of the past, but are still a challenge to locate and identify. As the rate of marine data collection increases, however, at ever higher resolutions, so grows the potential of this data to transform our understanding of the past. What is clear, therefore, is the need for methods which allow us to keep up with the rate of data generation, to help locate, and inform optimal recording and management strategies.

An area with a high density of recorded UCH is the continental shelf of the United Kingdom (UK) (Satchell and Palma, 2007). In English territorial waters alone (up to 12 nm), there are around 37,000 known shipwreck sites and recorded ship losses (England, 2016). The vast majority of the known historic maritime record in England dates from the mid-19th to mid-20th centuries, with 96% of known and dated wrecks lost between 1840 and 1950 (England, 2016). However, as recent research has highlighted, it is extremely difficult to quantify and identify this underwater resource accurately; a detailed assessment of 273 shipwrecks in the Irish Sea found that 40% of these 'known' wrecks

* Correspondence to: Department of Archaeology, Avenue Campus, Highfield Rd, Southampton, SO17 1BF, United Kingdom.
E-mail address: C.Pols@soton.ac.uk (C.T. Pols).

https://doi.org/10.1016/j.jas.2025.106297
Received 28 February 2025; Received in revised form 9 May 2025; Accepted 13 June 2025
Available online 5 July 2025

were misidentified (McCartney, 2022). The causes of misidentification were varied, but often related to the historically low resolution survey data that prevented clear identification of anything beyond anomaly, matched to heavy reliance on documentary evidence pointing to a location of loss, then equating the two. Thus, 'possible' equivalence slowly came to be read as 'probable'. These findings have significant implications for the wider study and understanding of shipwrecks in the UK. By extrapolating these results, it is estimated that at least 1,373 shipwrecks in the UK's Exclusive Economic Zone are currently misattributed (McCartney, 2022).

Thus, it becomes clear that there is an imperative to accurately locate and quantify UCH in order to begin to better understand what the record constitutes and how best to investigate and manage it. This desire extends beyond pure archaeological research as there is a variety of interested parties and stakeholders relating to seabed mapping; just in the UK alone, there are nine additional sectors that have equally valid interests in shipwrecks, which vary from fishing to navigation to recreation activities (Firth, 2018). However, in particular, the increasing amount of global offshore development, such as wind farms and underwater cables, can pose a more direct threat to shipwrecks (Papageorgiou, 2018).

Moreover, increasing offshore development, alongside the push for global seabed mapping (Jakobsson et al., 2017; Mayer et al., 2018; Wölfl et al., 2019) continues to generate large amounts of marine geophysical data that require assessment to identify underwater archaeological sites, such as shipwrecks. Archaeologists, therefore, require adequate methods, tools, and workflows to analyse these 'Big' datasets while remaining time, cost, and labour-effective in their identifications. Traditional analyst-led methods are becoming less desirable in the face of the sheer amount of geospatial data that require assessment. As such, semi-automated methods for the detection of potential sites is a growing interest in archaeological research (Opitz and Herrmann, 2018; Davis, 2019; Bickler, 2021; Cacciari and Pocobelli, 2022).

This paper aims to integrate two different semi-automated methods for the detection of shipwrecks on a regional scale using bathymetry (seabed elevation) data from the UK. The first method is a topographic inference approach, which identifies potential shipwrecks based on their value signatures in different raster data visualisations. The second method uses several machine learning algorithms trained to detect shipwrecks using different visualisations of bathymetry data. This includes a pre-trained detection model from ESRI (2021) as well as custom models created for this research. The performance of each method was evaluated against an existing shipwreck database (UKHO) and manual review.

The key contributions of this paper are:

- Provide an accessible and detailed workflow using traditional Geographic Information Systems (GIS) tools that identifies potential shipwrecks in large bathymetry datasets.
- Demonstrate the importance of careful application of semi-automated methods; specifically, how seabed variability needs to be accounted for to successfully apply machine learning methods in a precise manner.

2. Background

In recent years, the increase in volume, resolution, and access to wide-coverage remote sensing datasets has facilitated archaeological prospection at increasingly larger scales (Lambers et al., 2019). This so-called 'explosion' in digital spatial data has subsequently changed how archaeology is undertaken in many contexts (Bennett et al., 2014). The growing volume of digital data available also presents new challenges to current documentation workflows as traditional prospection methods become increasingly untenable at larger scales (Bevan, 2015; McCoy, 2017; Banaszek et al., 2018; Green, 2023). As such, there has been a push for closer integration of computer-aided detection in archaeological prospection (Bennett et al., 2014; Bevan, 2015; Traviglia et al., 2016).

2.1. Semi-automated methods for archaeological prospection

The use of computer-aided workflows has already enabled the development of image processing techniques for the rapid extraction of archaeological features in remote sensing imagery (Cheng and Han, 2016; Sevara et al., 2016). Previous computer-aided archaeological research used template matching to identify consistent geometric features (Lemmens et al., 1993; de Boer, 2005; Trier et al., 2009; Trier and Pilø, 2012; Kvamme, 2013), knowledge-based techniques to extract known sites such as enclosures (Zingman, 2016), and Object-Based Image Analysis (OBIA) to segment and classify images based on their visual properties (Bescoby, 2006; Van Ess et al., 2006; Jahjah et al., 2007; Hay and Castilla, 2008; Blaschke, 2010; Blaschke et al., 2014; Sevara and Pregesbauer, 2014; Magnini and Bettineschi, 2019; Janowski et al., 2021).

Template-matching and knowledge-based methods typically work well for regular, geometric features such as mounds, crop marks, and enclosures (Kvamme, 2013). However, these techniques are less adaptable and are not particularly suited for archaeological feature classes that have high variability in shape/size or that are rotationally variant (Kvamme, 2013). As such, OBIA methods have become more popular as they can overcome these limitations and have been increasingly applied to high-resolution geospatial data (Sevara and Pregesbauer, 2014; Davis, 2019).

In recent archaeological research, machine learning is also becoming increasingly popular as it has proven to be capable of classifying large and complex visual datasets for the detection of archaeological features (Caspari and Crespo, 2019, 2). Machine learning approaches differ from traditional methods because they do not explicitly rely on knowing the exact properties and characteristics of expected (archaeological) objects; rather than manually defining these properties to find objects that match given criteria, a computer learns these characteristics by being given positive and negative instances of an object class (Lambers et al., 2019, 3).

Despite their success, however, it is also clear that these techniques are arguably most effective when operating in parallel with, and under the supervision of, knowledgeable experts (Lucas, 2022; Hussain et al., 2023). Automated analysis can provide a useful first step in the recording process for areas that may lack a pre-existing historic record and, therefore, could provide a preliminary database for further development (Gallwey et al., 2019). Thus, machine learning can help realise the full potential of Big Data remote sensing datasets for archaeological purposes (Karamitrou et al., 2022) while keeping the 'human in the loop' element of traditional research. Moreover, even if just acting in a preliminary analytical capacity, machine learning facilitates the rapid identification of areas of greatest potential interest which can better target limited archaeological resources. In this manner, they can act as effective labour-saving tools as much as they are cost and time-effective (Lucas, 2022).

2.2. Machine learning in archaeology

For object identification in images, two main machine learning 'tasks' are used: object detection and image segmentation (Sevara et al., 2016). Overviews of the use of each these tasks are included in Tables 1, 2, and 3; while not exhaustive, they demonstrate broad trends within recent archaeological literature. Detailed and useful overviews of archaeological machine learning can be found elsewhere (Fiorucci et al., 2020; Mantovan and Nanni, 2020; Argyrou and Agapiou, 2022; Jamil et al., 2022; Kadhim and Abed, 2023; Câmara et al., 2023; Bellat et al., 2025) as well as more general overviews of machine learning in remote sensing (Guo et al., 2016; Ball et al., 2017; Garcia-Garcia et al., 2018; Minaee et al., 2020; Gui et al., 2024).

Object detection tasks have been frequently utilised in archaeological research as they are effective at localising potential features in large image datasets. These tasks have been primarily applied to satellite

Table 1
Table overview of object detection and image classification techniques in archaeological research.

Authors	Task	Algorithm	Data	Object(s)
Zingman et al. (2016)	Image Classification	AlexNet (CNN)	Satellite Imagery	Enclosures
Guyot et al. (2018)	Image Classification	Random Forests	LiDAR	Burial Mounds
Trier et al. (2018)	Image Classification	SVM, AlexNet	LiDAR	Charcoal Kilns
Caspari and Crespo (2019)	Image Classification	CNN	Satellite Imagery	Burial Mounds
Lambers et al. (2019)	Object Detection	WODAN (Faster R-CNN)	LiDAR	Barrows, Celtic Fields
Verschoof-van der Vaart and Lambers (2019)	Object Detection	WODAN (Faster R-CNN), VGG-16	LiDAR	Barrows, Celtic Fields, Charcoal Kilns
Trier et al. (2019)	Object Detection	CNN, ResNet-18	LiDAR	Roundhouses, Shieling Huts, Cairns
Orengo et al. (2020)	Image Classification	Random Forests	Multi-Spectral Imagery	Mounds
Phelan and Riordan (2020)	Image Classification	CNN, ResNet-34	Aerial Imagery	Ringforts
Somrak et al. (2020)	Image Classification	VGG-19	LiDAR	Aguada, Buildings, Platforms, Terrain
Kramer (2021)	Image Classification, Object Detection	CNN	LiDAR, Multi-Spectral Imagery	Various
Olivier and Verschoof-van der Vaart (2021)	Object Detection	YOLOv4	LiDAR	Barrows, Celtic Fields, Charcoal Kilns
Landauer et al. (2022)	Image Classification	CNN, ResNet-34	LiDAR	Hillforts
Canedo et al. (2023)	Object Detection	YOLOv5	LiDAR	Burial Mounds
Character et al. (2023)	Image Classification	Random Forests	LiDAR	Cave Entrances
Verschoof-van der Vaart et al. (2023)	Object Detection	YOLOv4	LiDAR	Relict Charcoal Hearths
Character et al. (2024)	Object Detection	YOLOv3	LiDAR	Mayan Mounds

imagery and LIDAR data and on a variety of site types; though they perform particularly well on regular feature classes such as barrows, mounds, and enclosures (Table 1).

Segmentation tasks are becoming increasingly popular because they offer a more complete understanding of an image scene through pixel-by-pixel labelling (Garcia-Garcia et al., 2018; Minaee et al., 2020). In recent archaeological research (Table 2), LiDAR data has used most frequently for image segmentation to detect a range of features (Kazimi et al., 2018; Gallwey et al., 2019; Kazimi et al., 2019; Bundzel et al., 2020; Bonhage et al., 2021; Guyot et al., 2021; Kazimi and Sester, 2023). Other data sources that have also been successfully used include satellite and aerial imagery (Soroush et al., 2020; Altaweel et al., 2022; Karamitrou et al., 2022), Ground Penetrating Radar (Küçükdemirci and Sarris, 2020), and even 3D photogrammetry datasets (Vandenabeele et al., 2023).

2.3. Machine learning in maritime archaeology

Machine learning approaches have also been successfully applied to several types of marine data for the detection of underwater sites and objects (Table 3). For example, object detection algorithms have been used for the identification of shipwrecks in side-scan sonar data (Ye et al., 2018; Xu et al., 2019; Zhu et al., 2019; Labbé-Morissette and Gautier, 2020; Xu et al., 2022). There has even been successful integration of these methods into real-time Autonomous Underwater Vehicle (AUV) surveys (Rutledge et al., 2018; Nayak et al., 2021), highlighting their potential for tackling global ocean mapping challenges (Wang et al., 2022).

Segmentation algorithms, however, have thus far been underutilised in maritime research, despite successful applications for amphorae detection in photo orthomosaics (Drap et al., 2019), shipwreck detection in satellite imagery (Karamitrou et al., 2023), and recent identification of seabed layers in sub-bottom seismic data (Fraser et al., 2024).

The closest comparable study for this research is Character et al.'s (2021) work using machine learning (object localisation) for shipwreck detection in bathymetry data from the United States. Their work provided a crucial proof-of-concept and demonstrated the capabilities of these methods for shipwreck detection; their model was able to detect 95% of the test shipwrecks while maintaining a very high precision rate of 90% across large areas of seabed (Character et al., 2021, 6-7).

3. Materials and methods

This study used publicly-accessible multibeam bathymetry data from the UK, downloaded through the Admiralty Seabed Mapping Service (available at: https://seabed.admiralty.co.uk). A spatial resolution of 1 m was used, based on previous research (Plets et al., 2011, 2), which identify this as being the minimum optimal resolution for shipwreck identification. The extent of the study area can be seen in Fig. 1, covering a total area of 15,126 km^2 from the North East to the South of England. All bathymetry data was in Bathymetry Attributed Grid (.bag) format, before conversion to TIFF (.tif), and each area downloaded corresponded to a single survey, rather than time average data. The individual bathymetry tiles were grouped into four major geographic regions: North East (NE), East (E), South East (SE), and South (S). This was done to enable easier handling of the data and reduce the computational requirements to process each layer.

An overview of the methods workflow, from data input to detection outputs, is shown in Fig. 2. All geospatial analysis, including the machine learning stage, was completed using ArcGIS Pro (3.3.0). The Deep Learning Libraries Framework for ArcGIS was required to run the necessary tools (available at: https://github.com/Esri/deep-learning-frameworks). The ArcGIS tools were subsequently run using an NVIDIA Quadro RTX 6000 GPU (NVIDIA-SMI 537.13) with 152 GB of GPU memory and NVIDIA CUDA (12.2). GPU use is recommended as it enables more efficient and faster image processing than the CPU (Hess and Alouta, 2021). The specific GIS tools used for each analysis step are italicised and/or in brackets (*Example Tool*).

Table 2
Table overview of image segmentation techniques in archaeological research.

Authors	Task	Algorithm	Data	Object(s)
Kazimi et al. (2018)	Image Segmentation	CNN, VGG-16, SAE	LiDAR	Natural Streams, Lakes, Tracks
Gallwey et al. (2019)	Image Segmentation	U-Net	LiDAR	Mining Pits
Kazimi et al. (2019)	Image Segmentation	DeepLabv3+	LiDAR	Bomb Craters, Charcoal Kilns
Bundzel et al. (2020)	Semantic Segmentation	U-Net, Mask R-CNN	LiDAR	Mayan Structures
Soroush et al. (2020)	Image Segmentation	U-Net	Satellite Imagery	Qanat Shafts
Küçükdemirci and Sarris (2020)	Semantic Segmentation	U-Net	GPR	Archaeological Structures (Buried)
Bonhage et al. (2021)	Instance Segmentation	Mask R-CNN	LiDAR	Relic Charcoal Hearths
Guyot et al. (2021)	Instance Segmentation	Mask R-CNN	LiDAR	Various
Altaweel et al. (2022)	Instance Segmentation	Mask R-CNN	UAV Aerial Imagery	Structures, Mounds, Qanats
Karamitrou et al. (2022)	Semantic Segmentation	SegNet, SimpleNet	Satellite Imagery	Arch. Features/ Structures
Kazimi and Sester (2023)	Semantic Segmentation	RVNet, RVGAN	LiDAR	Bomb Craters, Charcoal Kilns, Burial Mounds, Mining Holes
Vandenabeele et al. (2023)	Semantic Segmentation	DeepLabv3+	Photogrammetry	Historic Masonry

Table 3
Table overview of machine learning applications in maritime archaeology.

Authors	Task	Algorithm	Data	Object(s)
Rutledge et al. (2018)	Object Detection	SVM, CNN	Side-Scan Sonar	Shipwrecks
Ye et al. (2018)	Object Detection	VGG, ResNet18	Side-Scan Sonar	Shipwrecks, Aircraft
Nayak et al. (2021)	Object Detection	CNN	Side-Scan Sonar	Shipwrecks
Drap et al. (2019)	Image Segmentation	CNN	Underwater Imagery	Amphorae
Zhu et al. (2019)	Image Classification	AdaBoost, kNN, Random Forests, SVM	Side-Scan Sonar	Shipwrecks
Xu et al. (2019)	Object Detection	Faster R-CNN, YOLO, ImprovedNet	Side-Scan Sonar	Shipwrecks
Labbé-Morissette and Gautier (2020)	Object Detection	FAST, MSER, DBSCAN	Side-Scan Sonar	Shipwrecks, Fishing Gear
Character et al. (2021)	Object Detection	YOLOv3	Bathymetry	Shipwrecks
Xu et al. (2022)	Image Classification	SonarNet, GAPVGG (VGG16)	Side-Scan Sonar	Shipwrecks
Karamitrou et al. (2023)	Semantic Segmentation	SimpleNet	Satellite Imagery	Shipwrecks (Black Reefs)
Fraser et al. (2024)	Semantic Segmentation	DeepLabv3+	Seismic	Seabed Layers

3.1. Step 1: Raster extraction

The first semi-automated method identifies potential shipwrecks based on their influence on the seabed's topography (Fig. 3). This method was developed as a preliminary step to enhance and streamline the application of machine learning. Existing approaches typically rely on either geospatial techniques or machine learning independently, whereas this research integrates both, potentially offering a more effective application, as will be discussed later.

Shipwrecks cause changes to the seabed environment not only due to their material, e.g. metal wrecks (Karamitrou et al., 2023), but also due to their influence on the surrounding sediment and water dynamics (Quinn and Smyth, 2018). This method identifies areas of change on the seabed in the overlapping values of several different visualisation layers: slope, curvature, and topographic position index (TPI).

Slope and curvature were used because shipwrecks should have statistically different values in these visualisations compared to the background seabed topography (Character et al., 2021, 8). TPI values are a calculation of a cell's elevation compared to its surrounding neighbours within a specified range (Weiss, 2001; Jenness, 2006). This identifies areas of comparative high and low elevation (positive and negative TPI values, respectively). Thus TPI was used as it was well suited to identify not only shipwrecks themselves, which are often higher than the surrounding seabed, but also any scour that would be present (i.e. negative TPI). TPI was calculated with the Jenness (2006) method from the *Topography Toolbox for ArcGIS* (Dilts, 2019) and used a circle neighbourhood with a 30 cell radius (i.e. 30 metres). This was based on trial and error, attempting to maximise shipwreck signatures while minimising background topography.

To combine all three visualisations, the layers were reclassified into five classes using the *Reclassify* tool with the Jenks distribution function (ESRI, 2024). The Jenks distribution was used as it identifies natural groupings within a dataset that are not evenly distributed. Reclassification enables new values to be assigned to each class (i.e. range) of values. Slope was reclassified with low values being equal to 1 and high values being equal to 5 (Min-Max = 1,2,3,4,5), as we should expect shipwrecks to have higher slope values than the background seabed. Curvature and TPI were reclassified with both minimum and maximum values being equal to 5, then 4 then 1 (Min-Max = 5,4,1,4,5). This was done not only because high positive values of each of these layer should

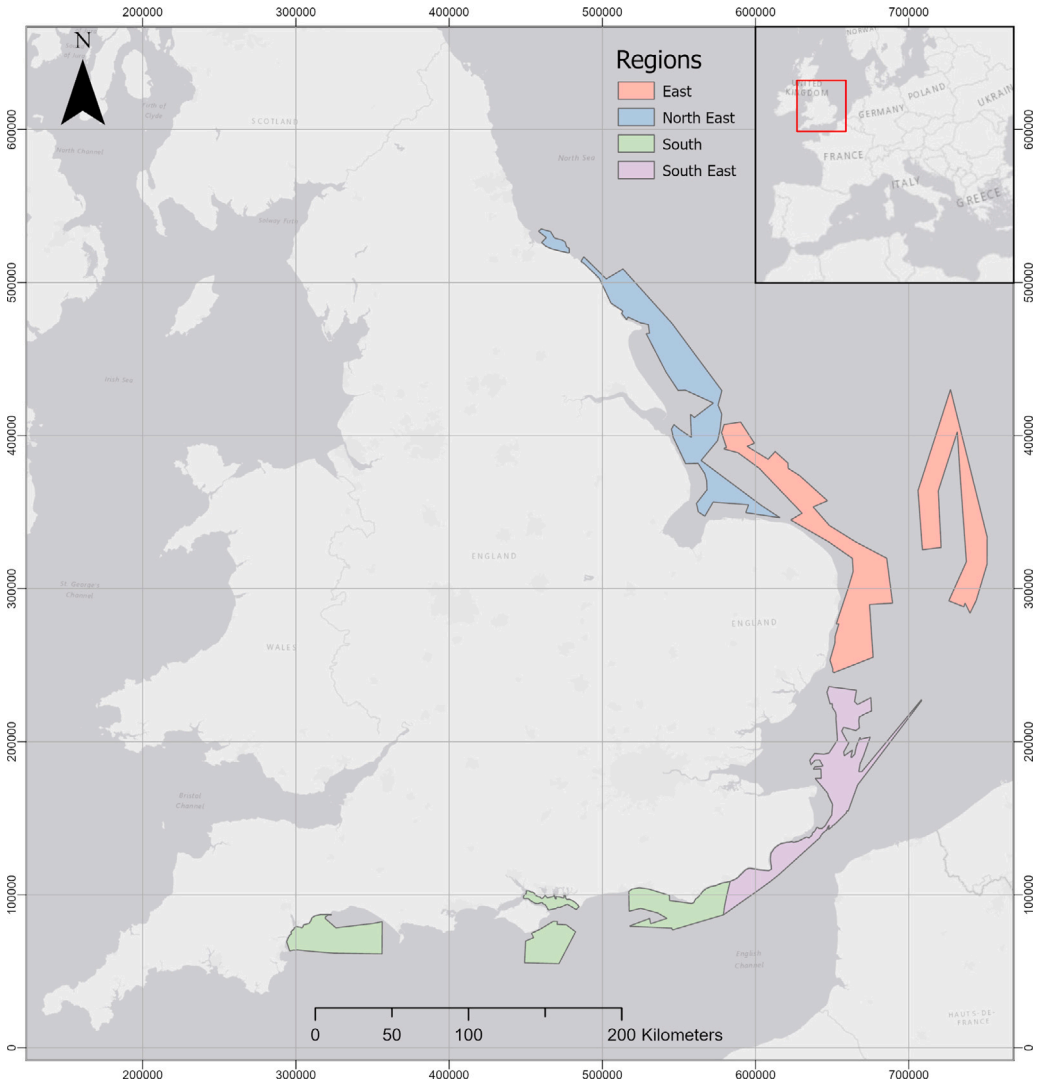

Fig. 1. Map showing the extent of 1 m bathymetry data used in this research. All data was downloaded from the Admiralty Seabed Mapping Service (available at: https://seabed.admiralty.co.uk). Map coordinates are shown in British National Grid.

indicate shipwrecks but also both negative curvature and TPI values can indicate seabed scour.

The visualisations were combined using the addition function in *Raster Calculator*, producing a single raster with a range of values between 3 and 15. By filtering out low value cells (*Extract by Attributes*) seabed areas with low shipwreck potential can be effectively removed and reduce the amount of data required for further assessment. For this research, only maximum cell values (15) were extracted in the combined raster, although a lower threshold (or a variable one) would also work. Finally, to produce a more workable format for manual review, the raster is converted into a polygon feature class (*Raster to Polygon*) and buffered to 20 m (*Buffer*) to reduce noise by merging detections with close spatial proximity.

The Raster Extraction workflow produces seabed areas with high potential for shipwreck sites, inferred from their topographic characteristics. These areas were then prepared for further analysis using machine learning detection models, trained to identify shipwrecks. To do this, centralised points for each output polygon were created (*Feature to Point*) and then buffered (*Buffer*) to the size of the trained models (256 × 256). Square polygons are then created using the *Minimum Bound Geometry* tool which are used to clip the visualisation layers (*Raster Clip*) used for detection input with the machine learning models.

3.2. Step 2: Machine learning in ArcGIS pro

All stages of the machine learning workflow (data collection, pre-processing, training, and testing) were completed using the deep learning tools available in ArcGIS Pro. ArcGIS was used because the software provides an accessible approach to machine learning tools while being easily integrated with geospatial datasets.

Several visualisation methods (hillshade, shaded relief, and curvature) were first used to increase the visibility of potential shipwreck sites from the original bathymetry. Hillshade is a standard visualisation in archaeological prospection studies and is often used in machine learning approaches. Shaded Relief is a type of colourised hillshade and was used to enable comparison to the pre-trained ESRI model (2021) which had been trained using this visualisation. The hillshade and shaded relief visualisations were created using default settings: Azimuth 315, Altitude 45, and Z factor 1.

Lastly, curvature was used because, while shipwrecks should have statistically different values in this visualisation compared to the surrounding seabed (Character et al., 2021, 8), it is not very easy to visually assess for the human analyst. Thus this enabled a comparison between 'analyst friendly' visualisations, hillshade and shaded relief, to a visualisation that may be more conducive to a computer vision approach.

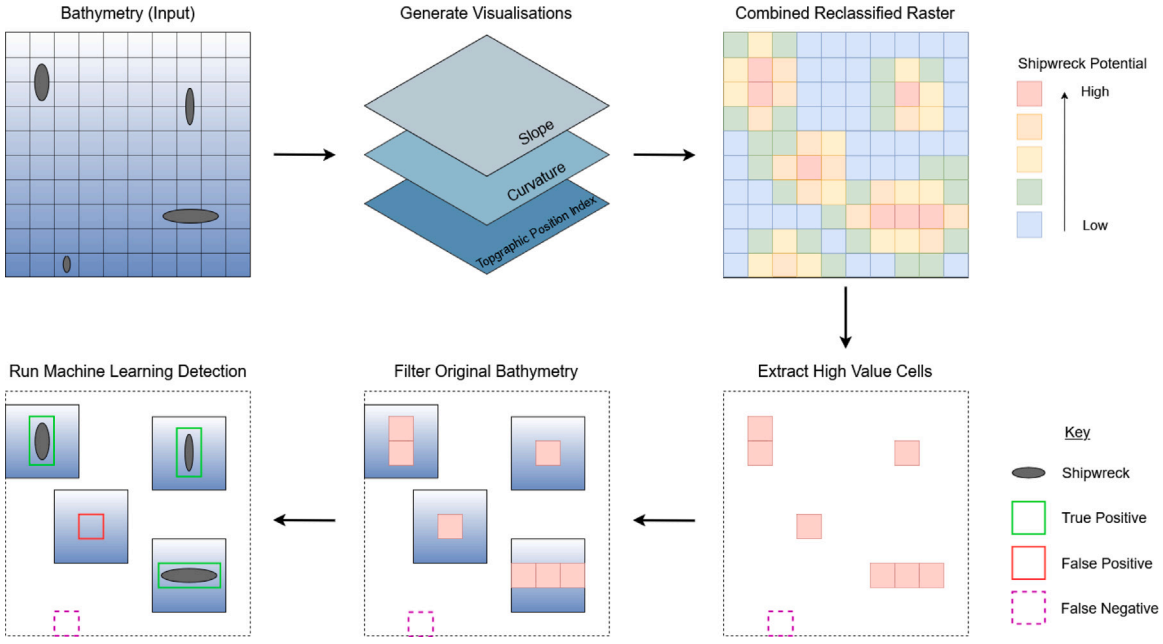

Fig. 2. A flowchart showing the overall methods workflow, from the bathymetry data input, visualisation creation, raster extraction filtering, and machine learning.

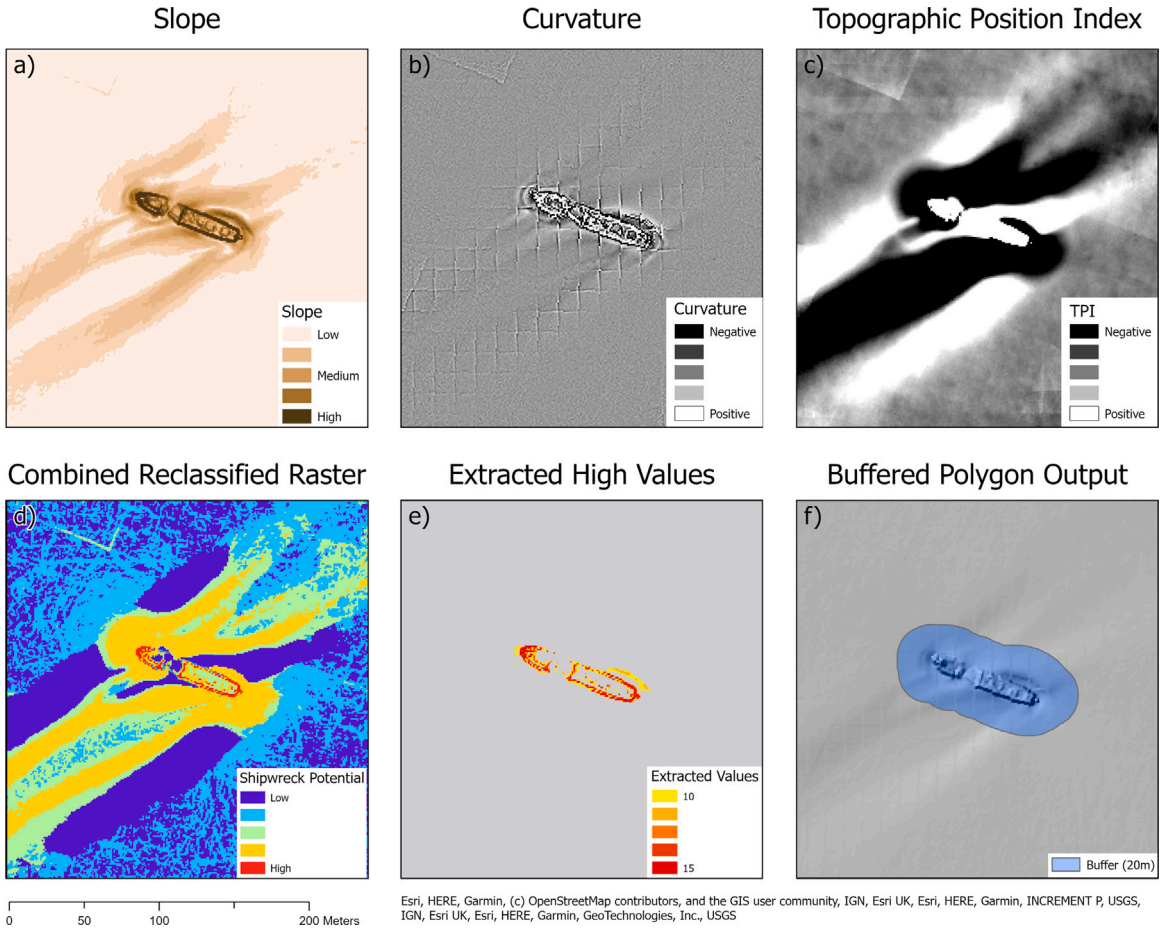

Fig. 3. The Raster Extraction workflow, showing the outputs of each stage: visualisations - (a) slope, (b) curvature, and (c) topographic position index. Analysis stage - (d) combined reclassified raster, (e) extracted high values (filtering), and (f) the final output as a buffered polygon (blue) shown with a hillshade background layer.

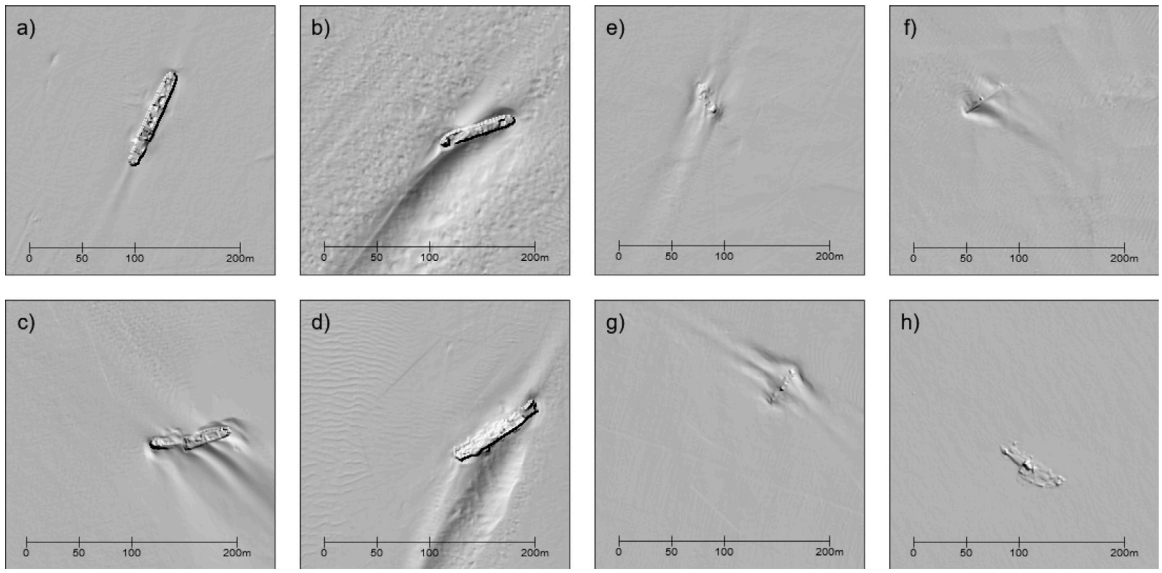

Fig. 4. Examples of hillshade training images used to train the hillshade detection models, showing the difference between conspicuous wrecks (left: a–d) and smaller, less visually prominent wreck sites (right: e–h).

3.2.1. Training data

Training data was created (*Export Training Data for Deep Learning*) which consisted of image tiles in TIFF (.tif) format of 256 × 256 pixel size. A single class of 'Shipwreck' was labelled and exported for the training data, which accounted for both conspicuous (i.e. well-preserved, highly visible) wrecks as well as smaller, possible wrecks (Fig. 4).

The training data was augmented primarily using 50% stride (128) and 90° image rotation to create synthetic data to increase the amount of training samples. In total 8,956 training images were created from 1,014 shipwrecks that were identified in the three training regions (NE, E, and SE). These images, while being labelled as a single object class, contained 573 examples of conspicuous shipwrecks and 441 examples of smaller wreck anomalies. Additional augmentation was completed during the training of the detection models (*Train Deep Learning Model*), which included further rotation, brightness, contrast, zoom, and crop changes (see Appendix, Table A.1).

3.2.2. Model architectures

Three different object detection models were selected in order to compare their performance for shipwreck detection. This enabled not only an evaluation of the impact of the different visualisations but also the machine learning algorithms themselves.

The first class of models used was 'Single Shot Detector' (SSD), a one-stage object detector that predicts object bounding boxes and class labels directly from the image (Liu et al., 2016). Without a proposal generation phase, SSD is fast and can even work in real-time settings. SSD algorithms can incorporate information from multiple scales, enabling them to detect objects of varying size (Liu et al., 2016).

Second, a Faster R-CNN (Region-based Convolutional Neural Network) model was used. In contrast to the SSD algorithm, this model has a two-stage object detection framework (Ren et al., 2016). The model's architecture is broken down into two modules: a Regions Proposal Network (RPN) and a Fast R-CNN feature extractor (Ren et al., 2016). Essentially, the RPN uses a CNN to propose regions of interest as a first stage and then a Fast R-CNN is used to extract features from the proposed regions.

The third model class, Mask R-CNN (used in the ESRI pre-trained model), is an extension of the Faster R-CNN algorithm which adds the capability of pixel-segmentation (He et al., 2017). This is a type of instance segmentation; in addition to the Faster R-CNN bounding box and class label, the Mask R-CNN generates a binary pixel mask for each object (He et al., 2017).

SSD models are specifically designed for object detection and have been used in previous archaeological studies (Ye et al., 2018; Verschoof-van der Vaart and Lambers, 2019; Trier et al., 2019). Several archaeological studies have also effectively used Faster R-CNN models (Verschoof-van der Vaart and Lambers, 2019; Trier et al., 2021) as well as the Mask R-CNN segmentation model (Bundzel et al., 2020; Altaweel et al., 2022; Bonhage et al., 2021; Guyot et al., 2021).

3.2.3. Backbone networks

All three model types were trained using the same backbone architecture of ResNet50. ResNet (Residual Network) is a type of CNN architecture that improves detection performance by making it easier to optimise (He et al., 2016). This is achieved by using residual (or skip) connections that allow the model to more efficiently learn through deeper layers.

The backbone architectures available in ArcGIS Pro have already been preconfigured (trained) on a generic image dataset, in this case, the ImageNet dataset (Russakovsky et al., 2015) to apply a procedure known as transfer learning. This is where a model trained on a particular task, typically a generic task with a large associated dataset, is fine-tuned on the task of interest. This process not only reduces the amount of training time required but research has shown that the use of pre-trained layer weights is greatly beneficial compared to random initialisation (Yosinski et al., 2014), including in remote sensing contexts (Nogueira et al., 2017).

Despite all other models and datasets performing well during training with ResNet50, the Faster R-CNN curvature model failed to learn. As such, another residual network, ResNet34, was used to train this model. Once the training stage was complete, the *Detect Object Using Deep Learning* tool was used to run the trained models across the testing area (see Appendix, Table A.2 for details).

4. Results

Using an existing shipwreck database (UKHO), a total of 253 shipwrecks were manually identified in the testing data (South region) across an area of around 3,131 km^2. These shipwrecks were grouped into two broad classes when evaluating the performance of each method; conspicuous (i.e. visually prominent) and 'possible' shipwrecks. The former consist of visually prominent wrecks that are

Table 4
Raster Extraction results for all shipwreck sites and conspicuous wrecks.

Raster Extraction		
Case 1: All Sites (n = 253)		
Recall	Precision	F1 Score
0.78	0.11	0.20
Case 2: Conspicuous Shipwrecks (n = 107)		
Recall	Precision	F1 Score
0.98	0.06	0.11

usually intact metal wrecks. The latter group was only able to be identified as wrecks using the UKHO database and typically were much smaller, less visually distinct sites.

Standard machine learning performance metrics, Recall, Precision, and F1 Score, were used to evaluate the performance of both the Raster Extraction method and the machine learning models. The basis of these measurements is the number of True Positives (TP), False Positives (FP), and False Negatives (FN) that are identified by the model.

Recall is the fraction of objects in the test data that are correctly identified (TP / (TP + FN)). Precision is the fraction of detections that are true positives (TP / (TP +FP)). F1 Score is the harmonic average of recall and precision that measures the detection performance for each selection class (F1 = 2 *x* recall *x* precision / (recall + precision)). These performance metrics are shown in Tables 4 and 5. The Raster Extraction method was able to identify 78% of all shipwrecks (197/253) in the testing area and performed particularly well on the conspicuous shipwrecks, with 98% (105/107) being detected. This method, however, had a low precision score; 11% for all features and only 6% for conspicuous wrecks, indicating high rates of false positive detections. The low F1 scores of the Raster Extraction (0.20 and 0.11) show that this method struggles to balance recall and precision.

In total, seven different machine learning (ML) detection models were trained and tested, each with interesting performance variations across networks and datasets. Examples of some of the true positives detections are shown in Fig. 6. The best-performing ML model on all shipwreck sites was an SSD trained on a curvature dataset, which identifies 73% of all sites with 47% precision. This is also reflected in the F1 score of 0.57, the highest for all the models, indicating the best balance between recall and precision. The best ML model for identifying conspicuous wrecks is an SSD trained on a shaded relief dataset which, despite a lower precision of 28%, detects 90% of these shipwrecks.

The ESRI pre-trained model was fine-tuned on the UK dataset as running the model without this step resulted in zero correct detections. The ESRI model was only able to detect just over half (55%) of all shipwreck sites, with a precision of 24%. It performed better on conspicuous wrecks, with 72% detected, although with a lower precision of 17%. The SSD trained on shaded relief had higher performance metrics for all sites and conspicuous wrecks than the ESRI model. Although the F-RCNN model had higher recall numbers, it had slightly lower precision and F1 scores than the ESRI model.

5. Discussion

5.1. Raster extraction

The Raster Extraction method filtered out 96% of the original test area, removing around 3,000 km^2, while still detecting 78% of all shipwreck sites. The vast majority of unidentified sites are in the 'possible' shipwreck class with only 63% of these sites being detected. However, 98% of conspicuous wrecks were successfully identified, with only two shipwrecks being missed (Fig. 5). As such, this method presents a strong use-case scenario for the rapid identification of prominent, metal wrecks in new survey data. Moreover, despite the low precision of this method, it functions well as a preliminary filtering step for the machine learning detection process, as it greatly reduces the amount of data that needs to be analysed while retaining a high recall score.

Research by Davis et al. (2020) and Davis et al. (2024) highlight the potential for using a more traditional, 'topographic inference' approach to identify both shipwrecks as well as smaller archaeological deposits. Davis et al. (2020) used a hydrological depression identification algorithm (Wu et al., 2016) and effectively repurposed it to detect possible shipwrecks in bathymetry data. Their Inverse Depression Analysis managed to achieve a recall of 71% in their study area.

This research attempted to extend this topographic inference approach by identifying potential shipwrecks not only by their elevational change but also by other characteristics (slope, curvature, TPI) which make them distinct features on the seabed. The use of three different visualisations has made this methodology more robust in its identifications; with a higher recall for all sites (78%) and was able to perform well across very large areas with different seabed environments. The implementation of this method is also relatively straightforward, using standard built-in GIS tools, making it an accessible way for rapid preliminary surveys.

While this method is very effective at reducing the amount of data, the low precision results shows that it works best in a preliminary capacity; further analysis, either using manual or machine learning methods, is required to reduce false positive detections. Also note that our workflow requires deciding on an appropriate value of a hyperparameter: the threshold value above which to consider the combined reclassified raster for detections. In this work, we set this to the maximum raster value (15). The existence of this hyperparameter could represent a limitation of our work, although it is common for detection algorithms to include such hyperparameters. However, using the maximum value did cause smaller, less prominent wreck sites to not be detected, reflected by only 63% of smaller sites being identified.

A key step to improve the Raster Extraction method and results would thus be to use a variable threshold based on a coarse-level seabed characterisation. By first completing a seabed characterisation, different thresholds could be optimised to different seabed environments. For example, using a lower threshold on flatter, sandy seabeds and higher threshold on more complex bedform areas. This step should further increase the amount of smaller shipwreck sites being detected but would also result in more overall detections (i.e. more false positives).

Existing semi-automated workflows for seabed classification using high-resolution bathymetry data already exist and have used both GIS-based approaches (Walbridge et al., 2018) as well as machine learning (Arosio et al., 2023). Seabed mapping is a multidisciplinary field, with importance to several different research areas including benthic ecology, marine geology, and subsea engineering. The Raster Extraction method could, therefore, be further developed into a more sophisticated workflow using tools and expertise developed in these fields.

5.2. Machine learning models

The machine learning models trained using Shaded Relief data consistently perform well in terms of recall, across both shipwreck classes, but often suffered from low precision. Curvature-based models (especially the SSD for all sites) achieve the highest precision and F1 scores, indicating a better balance between correct detections and false positives. This is particularly important because the curvature visualisation is not as analyst-friendly, i.e. easy to look at, than the other visualisations. The machine learning algorithms are unaffected by this, and even perform better on this dataset. Moreover, the most successful model network in terms of performance (SSD on curvature), is one of the worst performing models when trained and tested on hillshade data. Overall, precision remains low across most methods and datasets,

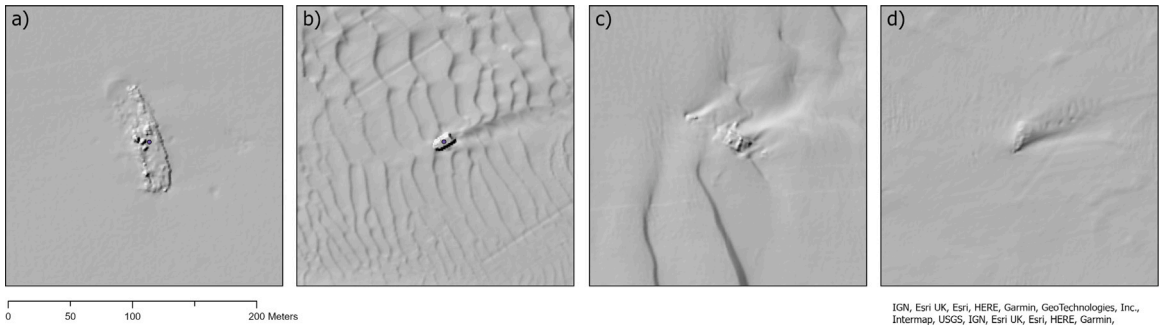

Fig. 5. Examples of shipwreck sites, shown in hillshade visualisation, that were not detected (False Negatives) by the raster extraction method: (a) and (b) are the two missed conspicuous wrecks, (c) a possible, disarticulated wreck, and (d) a small, possible wreck.

Table 5
Machine Learning results showing the performance of the custom models by algorithm (SSD, F-RCNN, and M-RCNN), visualisation, and shipwreck class. F-RCNN* indicates the only model trained with ResNet34 instead of ResNet50.

Visualisation	Hillshade		Curvature		Shaded Relief		ESRI
Model	F-RCNN	SSD	F-RCNN*	SSD	F-RCNN	SSD	M-RCNN
Case 1: All Features (n = 197)							
Recall	0.70	0.20	0.47	0.73	0.75	0.73	0.55
Precision	0.13	0.01	0.45	0.47	0.20	0.42	0.24
F1 Score	0.22	0.02	0.46	0.57	0.32	0.53	0.33
Case 2: Conspicuous Shipwrecks (n=105)							
Recall	0.90	0.21	0.70	0.85	0.90	0.90	0.72
Precision	0.09	0.01	0.36	0.29	0.13	0.28	0.17
F1 Score	0.16	0.01	0.48	0.43	0.23	0.43	0.27

reflecting a persistent issue with false positives. Models like the curvature F-RCNN and shaded relief SSD demonstrate some improvement, but may not be enough for consistently reliable classifications.

The ESRI model (after fine-tuning on the UK dataset) did not outperform other models that were pre-trained on generic image datasets. This may be because the characteristics of the original ESRI training data differ too much from the UK dataset. In the sample data the model is provided with, the ESRI model performs well on clusters of much smaller shipwrecks and has a reported average precision score of 0.92 in these conditions. In contrast, the UK dataset, and the test region specifically, typically has more isolated, larger shipwrecks. This difference is not optimal for transfer learning success, and thus there is currently no identifiable benefit of fine-tuning the ESRI model in these circumstances.

In Character et al.'s (2021) study they trained and tested a machine learning object detection model for shipwreck identification in hillshade visualisations of bathymetry data. Their model was able to achieve very high recall (95%) and precision (90%) across large a study area of seabed. Their work used fewer training images than this research, just 410 shipwreck chips, but was able to achieve substantially better results. The main difference, and the one likely limiting the precision of the custom detection models created here, is that they also trained their model on an equal number of background topography features to reduce the number of false positive detections. Character et al. (2021) also used a different model network and backbone algorithm (YOLOv3 with Darknet53; Redmon and Farhadi, 2018) than the models used in this research. Their research helps to, again, highlight the importance of considering the background seabed environment and its impact upon semi-automated methods. By integrating this background training to our models, the number of false positives is expected to reduce, especially if domain-specific knowledge is accounted for.

A regional breakdown of the detection results across the test area was completed to identify problematic areas causing false positives (Table 6). The table shows the top five largest numbers of detections across the test area regions for the Raster Extraction method and for each machine learning model. The tables shows a clear and consistent spatial pattern with several 'problematic' regions consistently causing high numbers of false positive detections for all methods and data visualisations. These problematic regions have large areas of rock outcrops, dense sand waves, and other linear seabed features that cause the erroneous detections (Fig. 7).

What is clear from this breakdown is that a major challenge to any semi-automated method is being able to adapt and overcome different levels of seabed complexity — from relatively flat, sandy seabeds to sand waves and exposed rock. Thus, the use of any method needs to have a clearly defined purpose for use and specification for what seabed environment it is suited to.

While recognising this challenge, there is still a reasonable opportunity for transferability of the detection models created during this research. It is feasible that these models could be applied to new high-resolution bathymetry datasets, both multibeam echosounder and LiDAR-derived bathymetry, to detect shipwrecks. Greater success is likely if higher spatial resolution data is used (e.g. 0.5 m) but larger wrecks would still be detected in slightly coarser data (e.g. 2 m).

5.3. Wider implications

In the context of the push for global seabed mapping and its corresponding Big Data challenges, it is clear that traditional manual interpretation techniques are becoming increasingly untenable. Automation helps offer a viable solution to effectively and systematically analysing vast (marine) datasets.

While it is true that conspicuous wrecks are typically easily identified during the data collection phase of marine geophysical surveys, manual detection of wrecks is subjective and highly influenced by factors like the processor's experience, fatigue, and time pressures. As such, automated tools can assist in identifying features that may have been missed during initial data processing, such as less-visually obvious, smaller shipwrecks. Moreover, with the increasing number of projects and the tight timelines for processing and interpreting data, semi-automated approaches are becoming crucial for double-checking and improving human interpretation.

Similarly, automated methods can also offer useful and effective ways to aid cultural heritage management strategies (Cowley, 2012; Magnini and Bettineschi, 2019). This is especially important for underwater cultural heritage, which can often be neglected or understudied

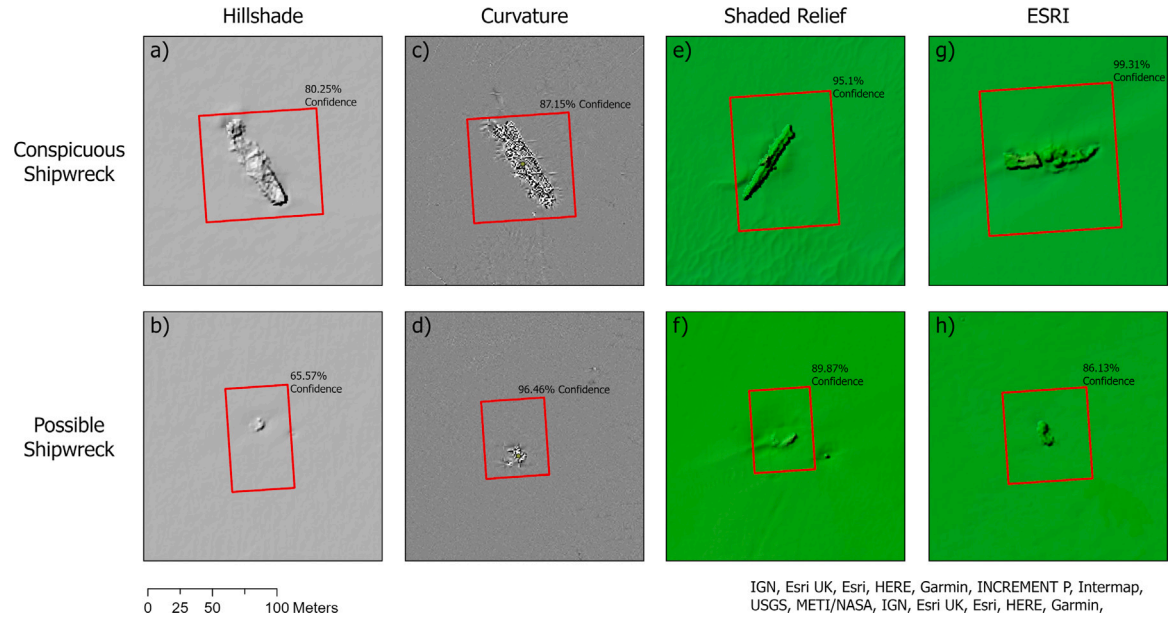

Fig. 6. Examples of True Positive machine learning detections on both conspicuous and smaller 'possible' shipwrecks. Results shown are from SSD models trained on hillshade (a,b), curvature (c,d), and shaded relief (e,f). Examples from the ESRI model (M R-CNN), trained on shaded relief, are also shown (g,h).

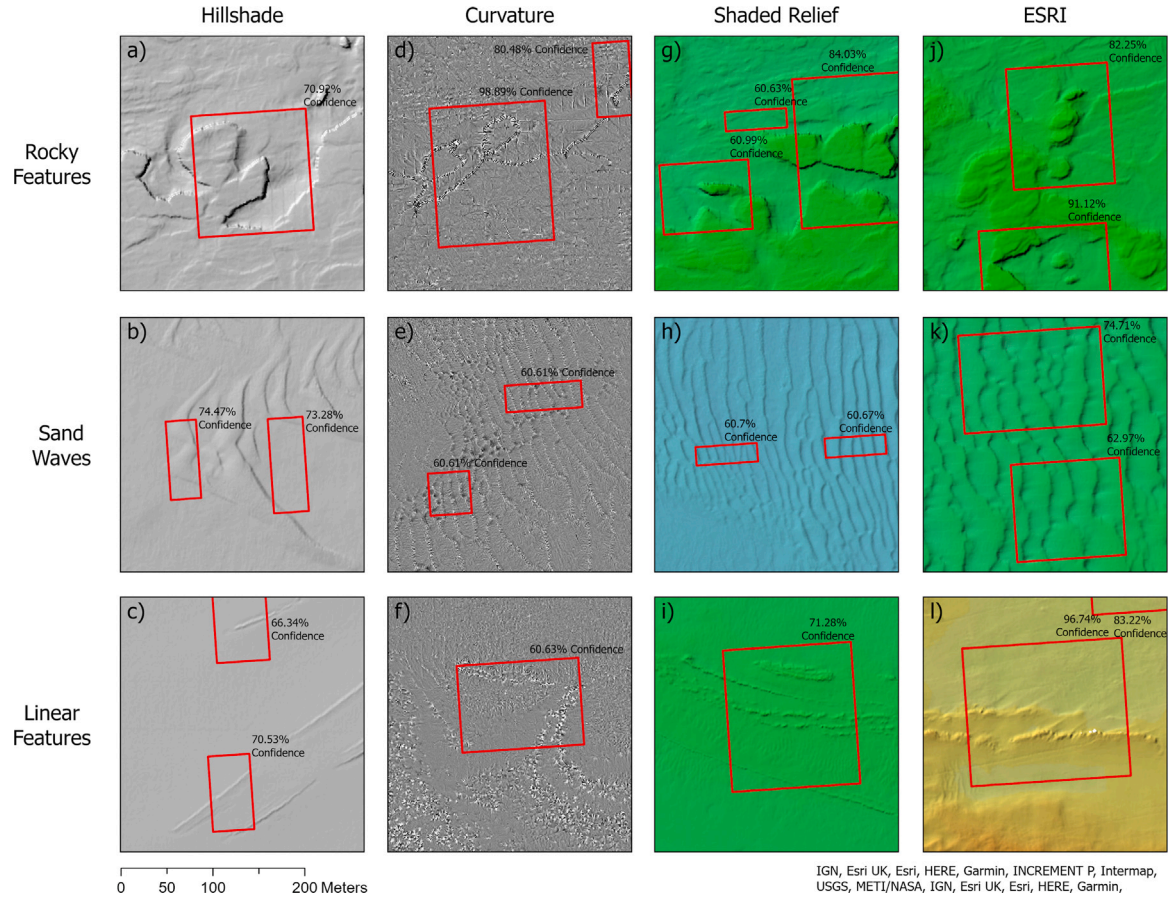

Fig. 7. Examples of False Positive machine learning detections, showing the main problematic features; rocky areas, sand waves, and linear features. Results shown are from SSD models trained on hillshade (a–c), curvature (d–f), and shaded relief (g–i). Examples from the ESRI model (Mask R-CNN), trained on shaded relief, are also shown (j–l).

Table 6
Regional breakdown of the survey areas that comprise the final testing area (South). This table shows the five largest numbers of detections across the survey regions by method and clearly identifies several commonly problematic areas.

Top 5 detection numbers								
	Raster Extraction	Hillshade		Curvature		Shaded Relief		ESRI
Region	Threshold 15	F-RCNN	SSD	F-RCNN	SSD	F-RCNN	SSD	M-RCNN
Lyme Bay 1N	x							
Lyme Bay 1S								
Lyme Bay 2								
Lyme Bay 3								
Lyme Bay 4				x				
Lyme Bay 5								
Selsey Bill to Lee-on-Solent	x	x	x	x	x	x		x
Southern Approaches Eastern Solent	x	x	x	x	x	x	x	x
Newhaven to Shoreham	x	x	x	x	x	x	x	
Beachy head to Newhaven Blk 1								x
Beachy head to Newhaven Blk 2							x	
Beachy Head East rMCZ	x	x	x		x	x	x	x
Hastings to Beachy Head		x	x	x	x	x	x	x
Percentage of All Detections	**94.5**	**80.0**	**55.6**	**84.43**	**65.85**	**73.53**	**61.03**	**83.97**

due to the challenges of the marine environment, such as inaccessibility (Andreou et al., 2022). New management strategies for underwater sites can be developed by using automated methods to rapidly identify areas of high archaeological potential through probable site identification, such as using the workflow outlined in this paper. This can be refined by using further classification of these detected sites, such as a shipwreck being articulated or disarticulated or using a more detailed class scheme (Gregory et al., 2024). From these classifications, priorities of study or conservation could be developed. In this manner, automated site detection and classification can thus also help inform field-based research and investigations, as has already been done for terrestrial research (Lambers, 2018).

6. Conclusions

This paper presents a new semi-automated workflow for the detection of shipwreck sites in bathymetric data. A preliminary 'topographic inference' approach was first applied to identify seabed areas with high shipwreck potential, based on their value signatures in three visualisations of bathymetry data: slope, curvature, and topographic position index (TPI). This Raster Extraction method acted as a filtering process, reducing the amount of data, prior to the application of machine learning (ML) object detection models. In total, seven different ML models were trained and tested for this research, which included testing three different algorithms (SSD, Faster R-CNN, and Mask R-CNN) combined with three different data visualisations: hillshade, curvature, and shaded relief. These methods were tested over 3,131 km^2 of 1 m resolution bathymetry from the south coast of England. In this area, a wide variety of shipwreck morphology had to be considered when evaluating the method performance; 'conspicuous' wrecks, defined as visually prominent, large shipwrecks as well as much smaller, possible wreck features.

The Raster Extraction method was able to filter 96% of the original test data while still detecting 78% of all shipwreck features (n = 197/253). It is particularly suited to identify conspicuous wrecks, with 98% of these being identified (n = 105/107). However, only 63% of smaller features were able to be detected as well as having a low precision rate overall (11%). The ML models that performed best on all sites were the curvature SSD (F1 = 0.57) and the shaded relief SSD (F1 = 0.53). For conspicuous wreck sites, 90% recall was achieved by three models (hillshade Faster R-CNN and shaded relief Faster R-CNN and SSD), although most models suffered from low precision.

This paper aimed to present this new workflow in an accessible format and used standard geospatial mapping tools to complete both stages of analysis in ArcGIS Pro. It also highlighted how the successful application of any semi-automated method for the detection of underwater archaeological sites needs to carefully consider the local seabed environment and the specific capabilities/limitations of the applied tools. These are particularly important considerations for archaeologists in the context of global seabed mapping initiatives to be able to effectively identify potential sites in rapidly expanding marine datasets.

CRediT authorship contribution statement

Cal T. Pols: Writing – review & editing, Writing – original draft, Visualization, Software, Methodology, Funding acquisition, Formal analysis, Conceptualization. **Fraser Sturt:** Writing – review & editing, Supervision, Methodology, Conceptualization. **Crystal El Safadi:** Writing – review & editing, Supervision, Methodology, Conceptualization. **Antonia Marcu:** Writing – review & editing, Supervision, Methodology, Conceptualization.

Declaration of competing interest

The authors declare the following financial interests/personal relationships which may be considered as potential competing interests: This research was funded by The Leverhulme Trust through the Southampton Marine and Maritime Institute (SMMI) as part of the Intelligence Oceans Doctoral Scholars program.

Acknowledgements

This research was funded by The Leverhulme Trust through the Southampton Marine and Maritime Institute (SMMI) as part of the Intelligence Oceans program. Cal Pols would like to thank Dr Felix Pedrotti for his insightful comments, feedback, and invaluable support.

All authors would like to thank the reviewers for their time and efforts to review this paper. We sincerely appreciate their feedback which improved both the clarity and quality of this work.

Appendix

Train Deep Learning Model tool parameters (Table A.1) and *Detect Object Using Deep Learning* tool parameters (Table A.2).

Data availability

All of the bathymetry data used in this study was downloaded from the Admiralty's Seabed Mapping Service available for free at: https://seabed.admiralty.co.uk/.

The UKHO Wrecks and Obstruction Database is available here: https://www.admiralty.co.uk/access-data/marine-data.

The Deep Learning Libraries Framework for ArcGIS is available at: https://github.com/Esri/deep-learning-frameworks.

Table A.1
Model training configuration.

Max Epochs	50
Model Type	SSD, Faster R-CNN, Mask R-CNN
Batch Size	64
Learning Rate	*Blank* (Optimal Learning Rate determined by ArcGIS based on learning curve)
Backbone Model	ResNet50 (*ResNet34 for Curvature F R-CNN)
Pre-trained Model	None (*Except for ESRI Mask R-CNN retrain)
Validation	10%
Stop when model stops improving	False (Continue Training)
Freeze Model	False (Unfreeze Model)
Data Augmentation	Custom
Augmentation Parameters	Rotate '30.0;0.5' Brightness '(0.4,0.6);1.0' Contrast '(0.75,1.5);1.0' Zoom '(1.0,1.2);1.0' Crop '224;1.0;(0,1);(0,1)'
Chip Size	256
Monitor Metric	Validation Loss

Table A.2
Model detection configuration.

Padding	56
Threshold	0.6
Batch Size	64
Exclude Pad Detections	True
Test Time Augmentation	False
Non Maximum Suppression	True
NMS Overlap	0.1
Confidence Score Field	Confidence
Max Overlap Ration	0
Processing Mode	Process as Mosaicked Image
Use Pixel Space	No Pixel Space

References

Adams, J., 2001. Ships and boats as archaeological source material. World Archaeol. 32 (3), 291–310.

Adams, J., 2013. A Maritime Archaeology of Ships. Oxbow Books, Oxford.

Altaweel, M., Khelifi, A., Li, Z., Squitieri, A., Basmaji, T., Ghazal, M., 2022. Automated archaeological feature detection using deep learning on optical UAV imagery: Preliminary results. Remote. Sens. 14 (3), 553. http://dx.doi.org/10.3390/rs14030553.

Andreou, G.M., Nikolaus, J., Westley, K., El Safadi, C., Blue, L., Smith, A., Breen, C., 2022. Big data in maritime archaeology: Challenges and prospects from the middle east and North Africa. J. Field Archaeol. 47 (3), 131–148. http://dx.doi.org/10.1080/00934690.2022.2028082.

Argyrou, A., Agapiou, A., 2022. A review of artificial intelligence and remote sensing for archaeological research. Remote. Sens. 14 (23), 6000. http://dx.doi.org/10.3390/rs14236000.

Arosio, R., Hobley, B., Wheeler, A.J., Sacchetti, F., Conti, L.A., Furey, T., Lim, A., 2023. Fully convolutional neural networks applied to large-scale marine morphology mapping. Front. Mar. Sci. 10, http://dx.doi.org/10.3389/fmars.2023.1228867.

Ball, J.E., Anderson, D.T., Chan, C.S., 2017. Comprehensive survey of deep learning in remote sensing: theories, tools, and challenges for the community. J. Appl. Remote. Sens. 11 (4), 042609. http://dx.doi.org/10.1117/1.JRS.11.042609.

Banaszek, L., Cowley, D.C., Middleton, M., 2018. Towards national archaeological mapping. assessing source data and methodology—A case study from Scotland. Geosciences 8 (8), 272. http://dx.doi.org/10.3390/geosciences8080272.

Basch, L., 1972. Ancient wrecks and the archaeology of ships. Int. J. Naut. Archaeol. 1 (1), 1–58.

Bellat, M., Figueroa, J.D.O., Reeves, J.S., Taghizadeh-Mehrjardi, R., Tennie, C., Scholten, T., 2025. Machine learning applications in archaeological practices: a review. http://dx.doi.org/10.48550/arXiv.2501.03840.

Bennett, R., Cowley, D., De Laet, V., 2014. The data explosion: tackling the taboo of automatic feature recognition in airborne survey data. Antiquity 88 (341), 896–905. http://dx.doi.org/10.1017/S0003598X00050766.

Bescoby, D.J., 2006. Detecting roman land boundaries in aerial photographs using radon transforms. J. Archaeol. Sci. 33 (5), 735–743. http://dx.doi.org/10.1016/j.jas.2005.10.012.

Bevan, A., 2015. The data deluge. Antiquity 89 (348), 1473–1484. http://dx.doi.org/10.15184/aqy.2015.102.

Bickler, S.H., 2021. Machine learning arrives in archaeology. Adv. Archaeol. Pr. 9 (2), 186–191. http://dx.doi.org/10.1017/aap.2021.6.

Blaschke, T., 2010. Object based image analysis for remote sensing. ISPRS J. Photogramm. Remote Sens. 65 (1), 2–16. http://dx.doi.org/10.1016/j.isprsjprs.2009.06.004.

Blaschke, T., Hay, G.J., Kelly, M., Lang, S., Hofmann, P., Addink, E., Queiroz Feitosa, R., van der Meer, F., van der Werff, H., van Coillie, F., Tiede, D., 2014. Geographic object-based image analysis – towards a new paradigm. ISPRS J. Photogramm. Remote Sens. 87, 180–191. http://dx.doi.org/10.1016/j.isprsjprs.2013.09.014.

Bonhage, A., Eltaher, M., Raab, T., Breuß, M., Raab, A., Schneider, A., 2021. A modified mask region-based convolutional neural network approach for the automated detection of archaeological sites on high-resolution light detection and ranging-derived digital elevation models in the North German Lowland. Archaeol. Prospect. 28 (2), 177–186. http://dx.doi.org/10.1002/arp.1806.

Bundzel, M., Jaščur, M., Kováč, M., Lieskovský, T., Sinčák, P., Tkáčik, T., 2020. Semantic segmentation of airborne LiDAR data in maya archaeology. Remote. Sens. 12 (22), 3685. http://dx.doi.org/10.3390/rs12223685.

Cacciari, I., Pocobelli, G.F., 2022. Machine learning: A novel tool for archaeology. In: D'Amico, S., Venuti, V. (Eds.), Handbook of Cultural Heritage Analysis. Springer International Publishing, Cham, pp. 961–1002. http://dx.doi.org/10.1007/978-3-030-60016-7_33.

Câmara, A., de Almeida, A., Caçador, D., Oliveira, J., 2023. Automated methods for image detection of cultural heritage: Overviews and perspectives. Archaeol. Prospect. 30 (2), 153–169. http://dx.doi.org/10.1002/arp.1883.

Canedo, D., Fonte, J., Seco, L.G., Vázquez, M., Dias, R., Pereiro, T.D., Hipólito, J., Menéndez-Marsh, F., Georgieva, P., Neves, A.J.R., 2023. Uncovering archaeological sites in airborne LiDAR data with data-centric artificial intelligence. IEEE Access 11, 65608–65619. http://dx.doi.org/10.1109/ACCESS.2023.3290305, Conference Name: IEEE Access.

Caspari, G., Crespo, P., 2019. Convolutional neural networks for archaeological site detection – finding "princely" tombs. J. Archaeol. Sci. 110, 104998. http://dx.doi.org/10.1016/j.jas.2019.104998.

Character, L., Beach, T., Inomata, T., Garrison, T.G., Luzzadder-Beach, S., Baldwin, J.D., Cambranes, R., Pinzón, F., Ranchos, J.L., 2024. Broadscale deep learning model for archaeological feature detection across the Maya area. J. Archaeol. Sci. 169, 106022. http://dx.doi.org/10.1016/j.jas.2024.106022.

Character, L., Beach, T., Luzzadder-Beach, S., Cook, D., Schank, C., Valdez Jr., F., Mallner, M., 2023. Machine learning for cave entrance detection in a Maya archaeological area. Phys. Geogr. 1–23. http://dx.doi.org/10.1080/02723646.2023.2261182.

Character, L., Ortiz JR, A., Beach, T., Luzzadder-Beach, S., 2021. Archaeologic machine learning for shipwreck detection using lidar and sonar. Remote. Sens. 13 (9), 1759. http://dx.doi.org/10.3390/rs13091759.

Cheng, G., Han, J., 2016. A survey on object detection in optical remote sensing images. ISPRS J. Photogramm. Remote Sens. 117, 11–28. http://dx.doi.org/10.1016/j.isprsjprs.2016.03.014.

Cowley, D.C., 2012. In with the new, out with the old? Auto-extraction for remote sensing archaeology. In: Remote Sensing of the Ocean, Sea Ice, Coastal Waters, and Large Water Regions 2012. 8532, SPIE, pp. 37–45. http://dx.doi.org/10.1117/12.981758.

Davis, D.S., 2019. Object-based image analysis: a review of developments and future directions of automated feature detection in landscape archaeology. Archaeol. Prospect. 26 (2), 155–163. http://dx.doi.org/10.1002/arp.1730.

Davis, D.S., Buffa, D.C., Wrobleski, A.C., 2020. Assessing the utility of open-access bathymetric data for shipwreck detection in the United States. Heritage 3 (2), 364–383. http://dx.doi.org/10.3390/heritage3020022.

Davis, D.S., Cook Hale, J.W., Hale, N.L., Johnston, T.Z., Sanger, M.C., 2024. Bathymetric lidar and semi-automated feature extraction assist underwater archaeological surveys. Archaeol. Prospect. 31 (2), 171–186. http://dx.doi.org/10.1002/arp.1939.

de Boer, A., 2005. Using pattern recognition to search LIDAR data for archeological sites. In: The World Is in Your Eyes. CAA2005. Computer Applications and Quantitative Methods in Archaeology. Proceedings of the 33rd Conference, Tomar, March 2005. CAA Portugal, Tomar, pp. 245–254, URL: https://proceedings.caaconference.org/paper/36_boer_caa_2005/.

Dilts, T.E., 2019. Topography tools for ArcGIS 10.3 and earlier - overview. URL: https://www.arcgis.com/home/item.html?id=b13b3b40fa3c43d4a23a1a09c5fe96b9.

Drap, P., Papini, O., Merad, D., Pasquet, J., Royer, J.-P., Motasem Nawaf, M., Saccone, M., Ben Ellefi, M., Chemisky, B., Seinturier, J., Sourisseau, J.-C., Gambin, T., Castro, F., 2019. Deepwater archaeological survey: An interdisciplinary and complex process. In: McCarthy, J.K., Benjamin, J., Winton, T., van Duivenvoorde, W. (Eds.), 3D Recording and Interpretation for Maritime Archaeology. In: Coastal Research Library, Springer International Publishing, Cham, pp. 135–153. http://dx.doi.org/10.1007/978-3-030-03635-5_9.

England, H., 2016. Ships and Boats: 1840 to 1950. Technical Report, HEAG133, Historic England, URL: https://historicengland.org.uk/images-books/publications/iha-ships-boats-1840-1950/.

ESRI, 2021. Shipwreck detection. URL: https://doc.arcgis.com/en/pretrained-models/latest/imagery/introduction-to-shipwreck-detection.htm.
ESRI, 2024. Data classification methods. URL: https://pro.arcgis.com/en/pro-app/latest/help/mapping/layer-properties/data-classification-methods.htm.
Fiorucci, M., Khoroshiltseva, M., Pontil, M., Traviglia, A., Del Bue, A., James, S., 2020. Machine learning for cultural heritage: A survey. Pattern Recognit. Lett. 133, 102–108, URL: https://doi.org/10.1016/j.patrec.2020.02.017.
Firth, A., 2018. Managing Shipwrecks. Honor Frost Trust, London.
Fraser, A.I., Landauer, J., Gaffney, V., Zieschang, E., 2024. Artificial interpretation: An investigation into the feasibility of archaeologically focused seismic interpretation via machine learning. Heritage 7 (5), 2491–2506. http://dx.doi.org/10.3390/heritage7050119.
Gallwey, J., Eyre, M., Tonkins, M., Coggan, J., 2019. Bringing lunar LiDAR back down to earth: Mapping our industrial heritage through deep transfer learning. Remote. Sens. 11 (17), 1994. http://dx.doi.org/10.3390/rs11171994.
Garcia-Garcia, A., Orts-Escolano, S., Oprea, S., Villena-Martinez, V., Martinez-Gonzalez, P., Garcia-Rodriguez, J., 2018. A survey on deep learning techniques for image and video semantic segmentation. Appl. Soft Comput. 70, 41–65. http://dx.doi.org/10.1016/j.asoc.2018.05.018.
Gibbins, D., Adams, J., 2001. Shipwrecks and maritime archaeology. World Archaeol. 32 (3), 279–291, URL: https://www.jstor.org/stable/827923.
Green, C., 2023. Big data in archaeology. In: Handbook of Archaeological Sciences. John Wiley & Sons, Ltd, pp. 1249–1259. http://dx.doi.org/10.1002/9781119592112.ch63.
Gregory, D., Dam, M., Majcher, J., Matthiesen, H., Andersen, G.N., Quinn, R., 2024. Using open-data portals, remote sensing and computational modelling to investigate historic wreck sites and their environments: 45 years on from Muckelroy. Int. J. Naut. Archaeol. 1–18. http://dx.doi.org/10.1080/10572414.2024.2320774.
Gui, S., Song, S., Qin, R., Tang, Y., 2024. Remote sensing object detection in the deep learning era—A review. Remote. Sens. 16 (2), 327. http://dx.doi.org/10.3390/rs16020327.
Guo, Y., Liu, Y., Oerlemans, A., Lao, S., Wu, S., Lew, M.S., 2016. Deep learning for visual understanding: A review. Neurocomputing 187, 27–48. http://dx.doi.org/10.1016/j.neucom.2015.09.116.
Guyot, A., Hubert-Moy, L., Lorho, T., 2018. Detecting neolithic burial mounds from LiDAR-derived elevation data using a multi-scale approach and machine learning techniques. Remote. Sens. 10 (2), 225. http://dx.doi.org/10.3390/rs10020225.
Guyot, A., Lennon, M., Lorho, T., Hubert-Moy, L., 2021. Combined detection and segmentation of archeological structures from LiDAR data using a deep learning approach. J. Comput. Appl. Archaeol. 4 (1), 1–19. http://dx.doi.org/10.5334/jcaa.64.
Hasslöf, O., 1972. The main principles in the technology of ship-building. In: Hasslöf, O., Henningsen, H., Christensen, A.E. (Eds.), Ships and Shipyards, Sailors and Fisherman: Introduction To Maritime Ethnology. Copenhagen University Press, Copenhagen, pp. 27–72.
Hay, G.J., Castilla, G., 2008. Geographic object-based image analysis (GEOBIA): A new name for a new discipline. In: Blaschke, T., Lang, S., Hay, G.J. (Eds.), Object-Based Image Analysis: Spatial Concepts for Knowledge-Driven Remote Sensing Applications. Springer, Cham, pp. 75–89.
He, K., Gkioxari, G., Dollár, P., Girshick, R., 2017. Mask R-CNN. In: 2017 IEEE International Conference on Computer Vision. ICCV, pp. 2980–2988. http://dx.doi.org/10.1109/ICCV.2017.322.
He, K., Zhang, X., Ren, S., Sun, J., 2016. Deep residual learning for image recognition. In: Proceedings of the IEEE Conference on Computer Vision and Pattern Recognition. pp. 770–778.
Hess, K., Alouta, R., 2021. Deep learning with arcgis pro tips & tricks: Part 1. ArcGIS Blog URL: https://www.esri.com/arcgis-blog/products/arcgis-pro/imagery/deep-learning-with-arcgis-pro-tips-tricks/.
Hussain, S.T., Riede, F., Plutniak, S., 2023. Automation and novelty –archaeocomputational typo-praxis in the wake of the third science revolution. Peer Community Archaeol. 1, 100307. http://dx.doi.org/10.24072/pci.archaeo.100307.
Jahjah, M., Ulivieri, C., Invernizzi, A., Parapetti, R., 2007. Archaeological remote sensing application pre-post war situation of babylon archaeological site—Iraq. Acta Astronaut. 61 (1), 121–130. http://dx.doi.org/10.1016/j.actaastro.2007.01.034.
Jakobsson, M., Allen, G., Carbotte, S.M., Falconer, R., Ferrini, V., Marks, K., 2017. The Nippon Foundation - GEBCO - Seabed 2030: Roadmap for Future Ocean Floor Mapping. Technical Report, GEBCO, URL: https://www.gebco.net/documents/seabed_2030_roadmap_v10_low.pdf.
Jamil, A.H., Yakub, F., Azizan, A., Roslan, S.A., Zaki, S.A., Ahmad, S.A., 2022. A review on deep learning application for detection of archaeological structures. J. Adv. Res. Appl. Sci. Eng. Technol. 26 (1), 7–14. http://dx.doi.org/10.37934/araset.26.1.714.
Janowski, L., Kubacka, M., Pydyn, A., Popek, M., Gajewski, L., 2021. From acoustics to underwater archaeology: Deep investigation of a shallow lake using high-resolution hydroacoustics—The case of lake Lednica, Poland. Archaeometry 63 (5), 1059–1080. http://dx.doi.org/10.1111/arcm.12663.
Jenness, J., 2006. Topographic Position Index (TPI). Jenness Enterprises, URL: http://www.jennessent.com/arcview/tpi.htm.
Kadhim, I., Abed, F.M., 2023. A critical review of remote sensing approaches and deep learning techniques in archaeology. Sensors 23 (6), 2918. http://dx.doi.org/10.3390/s23062918.
Karamitrou, A., Sturt, F., Bogiatzis, P., 2023. Identification of black reef shipwreck sites using AI and satellite multispectral imagery. Remote. Sens. 15 (8), 2030. http://dx.doi.org/10.3390/rs15082030.
Karamitrou, A., Sturt, F., Bogiatzis, P., Beresford-Jones, D., 2022. Towards the use of artificial intelligence deep learning networks for detection of archaeological sites. Surf. Topogr. Metrol. Prop. 10 (4), 044001. http://dx.doi.org/10.1088/2051-672X/ac9492.
Kazimi, B., Sester, M., 2023. Self-supervised learning for semantic segmentation of archaeological monuments in DTMs. J. Comput. Appl. Archaeol. 6 (1), 155–173. http://dx.doi.org/10.5334/jcaa.110.
Kazimi, B., Thiemann, F., Malek, K., Sester, M., Khoshelham, K., 2018. Deep learning for archaeological object detection in airborne laser scanning data. In: Belussi, A., Billen, R., Hallot, P., Migliorini, S. (Eds.), Proceedings of the 2nd Workshop on Computing Techniques for Spatio-Temporal Data in Archaeology and Cultural Heritage. In: CEUR Workshop Proceedings, vol. 2230, CEUR, Melbourne, Australia, pp. 21–35, URL: https://ceur-ws.org/Vol-2230/#paper_03.
Kazimi, B., Thiemann, F., Sester, M., 2019. Semantic segmentation of manmade landscape structures in digital terrain models. ISPRS Ann. Photogramm. Remote. Sens. Spat. Inf. Sci. IV-2-W7, 87–94. http://dx.doi.org/10.5194/isprs-annals-IV-2-W7-87-2019.
Kramer, I., 2021. Machine Learning for the Detection of Archaeological Sites from Remote Sensor Data (Ph.D. thesis). University of Southampton, Southampton.
Küçükdemirci, M., Sarris, A., 2020. Deep learning based automated analysis of archaeo-geophysical images. Archaeol. Prospect. 27 (2), 107–118. http://dx.doi.org/10.1002/arp.1763.
Kvamme, K.L., 2013. An examination of automated archaeological feature recognition in remotely sensed imagery. In: Bevan, A., Lake, M. (Eds.), Computational Approaches To Archaeological Spaces. Left Coast Press, Walnut Creek, pp. 53–68.
Labbé-Morissette, G., Gautier, S., 2020. Unsupervised extraction of underwater regions of interest in sidescan sonar imagery. J. Ocean. Technol. 15 (1), 95–108, URL: https://www.thejot.net/article-preview/?show_article_preview=1139.
Lambers, K., 2018. Airborne and spaceborne remote sensing and digital image analysis in archaeology. In: Siart, C., Forbriger, M., Bubenzer, O. (Eds.), Digital Geoarchaeology: New Techniques for Interdisciplinary Human-Environmental Research. In: Natural Science in Archaeology, Springer International Publishing, Cham, pp. 109–122. http://dx.doi.org/10.1007/978-3-319-25316-9_7.
Lambers, K., Verschoof-van der Vaart, W.B., Bourgeois, Q.P.J., 2019. Integrating remote sensing, machine learning, and citizen science in Dutch archaeological prospection. Remote. Sens. 11 (7), 794. http://dx.doi.org/10.3390/rs11070794.
Landauer, J., Hoppenstedt, B., Allgaier, J., 2022. Image segmentation to locate ancient maya architecture using deep learning. In: Kocev, D., Simidjievski, N., Kostovska, A., Dimitrovski, I., Kokalj, Z. (Eds.), Discover the Mysteries of the Maya. Jožef Stefan Institute, Ljubljana, pp. 7–12.
Lemmens, J.P.M.M., Stančič, Z., Verwaal, R.G., 1993. Automated archaeological feature extraction from digital aerial photographs. In: Andresen, J., Madsen, T., Scollar, I. (Eds.), Computing the Past. Computer Applications and Quantitative Methods in Archaeology CAA92. Aarhus University Press, Aarhus, pp. 45–52, URL: https://proceedings.caaconference.org/paper/03_lemmens_et_al_caa_1992/.
Liu, W., Anguelov, D., Erhan, D., Szegedy, C., Reed, S., Fu, C.-Y., Berg, A.C., 2016. SSD: Single shot MultiBox detector. In: Leibe, B., Matas, J., Sebe, N., Welling, M. (Eds.), Computer Vision – ECCV 2016. Springer International Publishing, Cham, pp. 21–37. http://dx.doi.org/10.1007/978-3-319-46448-0_2.
Lucas, G., 2022. Archaeology, Typology and Machine Epistemology. Technical Report, Zenodo, http://dx.doi.org/10.5281/zenodo.7622162.
Magnini, L., Bettineschi, C., 2019. Theory and practice for an object-based approach in archaeological remote sensing. J. Archaeol. Sci. 107, 10–22. http://dx.doi.org/10.1016/j.jas.2019.04.005.
Mantovan, L., Nanni, L., 2020. The computerization of archaeology: Survey on artificial intelligence techniques. SN Comput. Sci. 1 (5), 267. http://dx.doi.org/10.1007/s42979-020-00286-w.
Mayer, L., Jakobsson, M., Allen, G., Dorschel, B., Falconer, R., Ferrini, V., Lamarche, G., Snaith, H., Weatherall, P., 2018. The nippon foundation—GEBCO seabed 2030 project: The quest to see the world's oceans completely mapped by 2030. Geosciences 8 (2), 63. http://dx.doi.org/10.3390/geosciences8020063.
McCartney, I., 2022. Echoes from the Deep. Inventorising Shipwrecks at the National Scale by the Application of Marine Geophysics and the Historical Text. Sidestone Press, URL: https://www.sidestone.com/books/echoes-from-the-deep.
McCoy, M.D., 2017. Geospatial big data and archaeology: Prospects and problems too great to ignore. J. Archaeol. Sci. 84, 74–94. http://dx.doi.org/10.1016/j.jas.2017.06.003.
Minaee, S., Boykov, Y., Porikli, F., Plaza, A., Kehtarnavaz, N., Terzopoulos, D., 2020. Image segmentation using deep learning: A survey. http://dx.doi.org/10.48550/arXiv.2001.05566, URL: http://arxiv.org/abs/2001.05566.
Muckelroy, K., 1978. Maritime Archaeology. Cambridge University Press, Cambridge.
Nayak, N., Nara, M., Gambin, T., Wood, Z., Clark, C.M., 2021. Machine learning techniques for AUV side-scan sonar data feature extraction as applied to intelligent search for underwater archaeological sites. In: Ishigami, G., Yoshida, K. (Eds.), Field Serv. Robot. 16, 219–233. http://dx.doi.org/10.1007/978-981-15-9460-1_16.
Nogueira, K., Penatti, O.A.B., dos Santos, J.A., 2017. Towards better exploiting convolutional neural networks for remote sensing scene classification. Pattern Recognit. 61, 539–556. http://dx.doi.org/10.1016/j.patcog.2016.07.001.

Olivier, M., Verschoof-van der Vaart, W., 2021. Implementing state-of-the-art deep learning approaches for archaeological object detection in remotely-sensed data: The results of cross-domain collaboration. J. Comput. Appl. Archaeol. 4 (1), 274–289. http://dx.doi.org/10.5334/jcaa.78.

Opitz, R., Herrmann, J., 2018. Recent trends and long-standing problems in archaeological remote sensing. J. Comput. Appl. Archaeol. 1 (1), 19. http://dx.doi.org/10.5334/jcaa.11.

Orengo, H.A., Conesa, F.C., Garcia-Molsosa, A., Lobo, A., Green, A.S., Madella, M., Petrie, C.A., 2020. Automated detection of archaeological mounds using machine-learning classification of multisensor and multitemporal satellite data. Proc. Natl. Acad. Sci. 117 (31), 18240–18250. http://dx.doi.org/10.1073/pnas.2005583117.

Papageorgiou, M., 2018. Underwater cultural heritage facing maritime spatial planning: Legislative and technical issues. Ocean & Coastal Management 165, 195–202. http://dx.doi.org/10.1016/j.ocecoaman.2018.08.032.

Phelan, K., Riordan, D., 2020. Detection of ringforts from aerial photography using machine learning. In: 2020 31st Irish Signals and Systems Conference. ISSC, pp. 1–6. http://dx.doi.org/10.1109/ISSC49989.2020.9180159.

Plets, R., Quinn, R., Forsythe, W., Westley, K., Bell, T., Benetti, S., McGrath, F., Robinson, R., 2011. Using multibeam echo-sounder data to identify shipwreck sites: archaeological assessment of the joint Irish bathymetric survey data. Int. J. Naut. Archaeol. 40 (1), 87–98. http://dx.doi.org/10.1111/j.1095-9270.2010.00271.x.

Quinn, R., Smyth, T.A.G., 2018. Processes and patterns of flow, erosion, and deposition at shipwreck sites: a computational fluid dynamic simulation. Archaeol. Anthr. Sci. 10 (6), 1429–1442. http://dx.doi.org/10.1007/s12520-017-0468-7.

Redmon, J., Farhadi, A., 2018. YOLOv3: An incremental improvement. http://dx.doi.org/10.48550/arXiv.1804.02767.

Ren, S., He, K., Girshick, R., Sun, J., 2016. Faster R-CNN: Towards real-time object detection with region proposal networks. http://dx.doi.org/10.48550/arXiv.1506.01497.

Russakovsky, O., Deng, J., Su, H., Krause, J., Satheesh, S., Ma, S., Huang, Z., Karpathy, A., Khosla, A., Bernstein, M., Berg, A.C., Fei-Fei, L., 2015. ImageNet large scale visual recognition challenge. Int. J. Comput. Vis. (IJCV) 115 (3), 211–252. http://dx.doi.org/10.1007/s11263-015-0816-y.

Rutledge, J., Yuan, W., Wu, J., Freed, S., Lewis, A., Wood, Z., Gambin, T., Clark, C., 2018. Intelligent shipwreck search using autonomous underwater vehicles. In: 2018 IEEE International Conference on Robotics and Automation. ICRA, pp. 6175–6182. http://dx.doi.org/10.1109/ICRA.2018.8460548.

Satchell, J., Palma, P., 2007. Managing the marine cultural heritage: Defining, accessing and managing the resource (ed). In: Satchell, J., Palma, P. (Eds.), Managing the Marine Cultural Heritage: Defining, Accessing and Managing the Resource. URL: https://www.academia.edu/5813196/Managing_the_Marine_Cultural_Heritage_Defining_Accessing_and_Managing_the_Resource_ed_.

Sevara, C., Pregesbauer, M., 2014. Archaeological feature classification: An object orientated approach. South East. Eur. J. Earth Obs. Geomatics 3 (2S), 139–144.

Sevara, C., Pregesbauer, M., Doneus, M., Verhoeven, G., Trinks, I., 2016. Pixel versus object — A comparison of strategies for the semi-automated mapping of archaeological features using airborne laser scanning data. J. Archaeol. Sci. Rep. 5, 485–498. http://dx.doi.org/10.1016/j.jasrep.2015.12.023.

Somrak, M., Džeroski, S., Kokalj, Z., 2020. Learning to classify structures in ALS-derived visualizations of ancient maya settlements with CNN. Remote. Sens. 12 (14), 2215. http://dx.doi.org/10.3390/rs12142215.

Soroush, M., Mehrtash, A., Khazraee, E., Ur, J.A., 2020. Deep learning in archaeological remote sensing: Automated qanat detection in the Kurdistan region of Iraq. Remote. Sens. 12 (3), 500. http://dx.doi.org/10.3390/rs12030500.

Traviglia, A., Cowley, D., Lambers, K., 2016. Finding common ground: human and computer vision in archaeological prospection. AARGnews Newsl. Aer. Archaeol. Res. Group 53, 11–24, URL: https://hdl.handle.net/1887/43751.

Trier, O.D., Cowley, D.C., Waldeland, A.U., 2019. Using deep neural networks on airborne laser scanning data: Results from a case study of semi-automatic mapping of archaeological topography on arran, Scotland. Archaeol. Prospect. 26 (2), 165–175. http://dx.doi.org/10.1002/arp.1731.

Trier, O.D., Larsen, S.O., Solberg, R., 2009. Automatic detection of circular structures in high-resolution satellite images of agricultural land. Archaeol. Prospect. 16 (1), 1–15. http://dx.doi.org/10.1002/arp.339.

Trier, O.D., Pilø, L.H., 2012. Automatic detection of pit structures in airborne laser scanning data. Archaeol. Prospect. 19 (2), 103–121. http://dx.doi.org/10.1002/arp.1421.

Trier, O.D., Reksten, J.H., Løseth, K., 2021. Automated mapping of cultural heritage in Norway from airborne lidar data using faster R-CNN. Int. J. Appl. Earth Obs. Geoinf. 95, 102241. http://dx.doi.org/10.1016/j.jag.2020.102241.

Trier, O.D., Salberge, A.B., Pilø, L.H., 2018. Semi-automatic mapping of charcoal kilns from airborne laser scanning data using deep learning. In: CAA2016: Oceans of Data. Proceedings of the 44th Conference on Computer Applications and Quantitative Methods in Archaeology. Archaeo Press, Oxford, pp. 219–231.

UNESCO, 2001. Convention on the Protection of the Underwater Cultural Heritage. Technical Report, United Nations, URL: https://unesdoc.unesco.org/ark:/48223/pf0000126065.

UNESCO, 2007. Convention on the protection of the underwater cultural heritage. In: Programme and Meeting Document CLT/CIH/MCO/2007/PI/38. UNESCO, Paris, pp. 1–32, URL: https://unesdoc.unesco.org/ark:/48223/pf0000152883.

Verschoof-van der Vaart, W., Bonhage, A., Schneider, A., Ouimet, W., Raab, T., 2023. Automated large-scale mapping and analysis of relict charcoal hearths in connecticut (USA) using a deep learning YOLOv4 framework. Archaeol. Prospect. 30 (3), 251–266. http://dx.doi.org/10.1002/arp.1889.

Verschoof-van der Vaart, W.B., Lambers, K., 2019. Learning to look at LiDAR: The use of R-CNN in the automated detection of archaeological objects in LiDAR data from the Netherlands. J. Comput. Appl. Archaeol. 2 (1), 31–40. http://dx.doi.org/10.5334/jcaa.32.

Van Ess, M., Becker, H., Fassbinder, J., Kiefl, R., Lingenfelder, I., Schreier, G., Zevenbergen, A., 2006. Detection of looting activities at archaeological sites in Iraq using ikonos imagery. In: Strobl, J., Blaschke, T., Griesebner, G. (Eds.), In: Angewandte Geoinformatik; BeitrÄge Zum, vol. 18, Wiechmann-Verlag, Heidelberg, pp. 668–678.

Vandenabeele, L., Loverdos, D., Pfister, M., Sarhosis, V., 2023. Deep learning for the segmentation of large-scale surveys of historic masonry: A new tool for building archaeology applied at the Basilica of St Anthony in Padua. Int. J. Archit. Herit. 1–13. http://dx.doi.org/10.1080/15583058.2023.2260771.

Walbridge, S., Slocum, N., Pobuda, M., Wright, D.J., 2018. Unified geomorphological analysis workflows with benthic terrain modeler. Geosciences 8 (3), 94. http://dx.doi.org/10.3390/geosciences8030094.

Wang, N., Wang, Y., Er, M.J., 2022. Review on deep learning techniques for marine object recognition: Architectures and algorithms. Control Eng. Pract. 118, 104458. http://dx.doi.org/10.1016/j.conengprac.2020.104458.

Weiss, A., 2001. Topographic Position and Landforms Analysis. San Diego, CA, URL: https://env761.github.io/assets/files/tpi-poster-tnc_18x22.pdf.

Wölfl, A.-C., Snaith, H., Amirebrahimi, S., Devey, C.W., Dorschel, B., Ferrini, V., Huvenne, V.A.I., Jakobsson, M., Jencks, J., Johnston, G., Lamarche, G., Mayer, L., Millar, D., Pedersen, T.H., Picard, K., Reitz, A., Schmitt, T., Visbeck, M., Weatherall, P., Wigley, R., 2019. Seafloor mapping – the challenge of a truly global ocean bathymetry. Front. Mar. Sci. 6, URL: https://www.frontiersin.org/articles/10.3389/fmars.2019.00283.

Wu, Q., Deng, C., Chen, Z., 2016. Automated delineation of karst sinkholes from LiDAR-derived digital elevation models. Geomorphology 266, 1–10. http://dx.doi.org/10.1016/j.geomorph.2016.05.006.

Xu, L., Wang, X., Wang, X., 2019. Shipwrecks detection based on deep generation network and transfer learning with small amount of sonar images. In: 2019 IEEE 8th Data Driven Control and Learning Systems Conference. DDCLS, IEEE, pp. 638–643. http://dx.doi.org/10.1109/DDCLS46542.2019.

Xu, H., Yang, L., Long, X., 2022. Underwater sonar image classification with small samples based on parameter-based transfer learning and deep learning. In: 2022 Global Conference on Robotics, Artificial Intelligence and Information Technology. GCRAIT, pp. 304–307. http://dx.doi.org/10.1109/GCRAIT55928.2022.00071.

Ye, X., Li, C., Zhang, S., Yang, P., Li, X., 2018. Research on side-scan sonar image target classification method based on transfer learning. In: OCEANS 2018 MTS/IEEE Charleston. pp. 1–6. http://dx.doi.org/10.1109/OCEANS.2018.8604691.

Yosinski, J., Clune, J., Bengio, Y., Lipson, H., 2014. How transferable are features in deep neural networks? Adv. Neural Inf. Process. Syst. 3320–3328. http://dx.doi.org/10.48550/arXiv.1411.1792.

Zhu, B., Wang, X., Chu, Z., Yang, Y., Shi, J., 2019. Active learning for recognition of shipwreck target in side-scan sonar image. Remote. Sens. 11 (3), 243. http://dx.doi.org/10.3390/rs11030243.

Zingman, I., 2016. Semi-Automated Detection of Fragmented Rectangular Structures in High Resolution Remote Sensing Images with Application in Archaeology (Ph.D. thesis). Universität Konstanz, URL: https://kops.uni-konstanz.de/handle/123456789/36650.

Zingman, I., Saupe, D., Penatti, O.A.B., Lambers, K., 2016. Detection of fragmented rectangular enclosures in very high resolution remote sensing images. IEEE Trans. Geosci. Remote Sens. 54 (8), 4580–4593.